Case Report: High-Resolution Simultaneous Multi-Slice (SMS) RESOLVE Diffusion Neurography for Evaluation of Peripheral Nerve Entrapment Syndrome and Neuropathy

Andreas J. Bartsch[1,2,3]

[1] Radiologie Bamberg, Germany
[2] Depts. of Neuroradiology, Universities of Heidelberg and Wuerzburg, Germany
[3] Oxford Centre for Functional MRI of the Brain (FMRIB), University of Oxford, UK

Abstract

Diffusion echo-planar imaging (EPI) using read-out segmentation of long variable echo trains (RESOLVE; [1]) has primarily been developed for high-resolution diffusion-weighted imaging with reduced susceptibility-based geometric image distortions as well as T2*-decay related blurring and robust correction for motion-induced phase artifacts. Notably, RESOLVE also reduces the echo time (TE) but increases the scan time of the acquisitions.

Simultaneous multi-slice (SMS) imaging has initiated a "new revolution" of accelerated MRI scanning [2], particularly for EPI. For diffusion EPI investigating structures with non-uniformly directed diffusion and areas of crossing fibers, like in the central nervous system, SMS principally allows to sample more diffusion directions and shells within a given acquisition time. In the peripheral nervous system with rather uniformly directed diffusion and few crossing fibers, however, substantial gains offered by SMS may be primarily related to increases in spatial image resolution and lower slice thicknesses. Thin slices reduce partial volume artifacts and facilitate isotropic recordings while an increased number of slices is able to maintain or extend the coverage.

As yet, SMS has primarily gained attention for brain examinations while RESOLVE has also been applied to extracranial (such as head-and-neck cancer) imaging. Here we illustrate the utility of high-resolution SMS RESOLVE[1] diffusion neurography for evaluation of peripheral neuropathies, exemplified by ulnar nerve compression at the Loge de Guyon.

Patient history

A 59-year-old left-handed woman presented with brachialgia paraesthetica nocturna of the left hand. It had developed about two months ago and consecutively worsened. She had been using a crutch due to severe, activated coxarthrosis on the left for six months and was originally transferred for MR evaluation of presumed carpal tunnel syndrome (median compression neuropathy).

Clinical examination revealed slight sensory loss of the left palmar hypothenar but not the thenar area. Phalen's maneuver was negative on both sides while Froment's sign was slightly positive on the left. Tapping the ulnar nerve at the level of the Loge de Guyon provoked paraesthesias of the fifth and the ulnar side of the fourth digit (positive Tinel's sign).

[1] The product is still under development and not commercially available yet. Its future availability cannot be ensured.

There was slight left adductor- but also opponens-pollicis-weakness, compared to the right non-dominant hand, as manifested in the strength (4 out of 5) of key grip and thumb opposition. No muscular atrophy was detected, and fist closing was symmetric, with no claw hand. The thumb-to-little-finger and Schaeffer's tests were intact.

Imaging sequence and post-processing details

Imaging was performed on a 3 Tesla MAGNETOM Skyra scanner (Siemens Healthcare, Erlangen, Germany) running on software version *syngo*.MR E11C and using a 16-channel wrist coil.

Axial coplanar diffusion-, T2- as well as proton-density- and T1-weighted 2D-sequences were recorded, each with 30 slices at a slice thickness of 2.50 mm and a 10% interslice gap. For the relevant diagnostic diffusion- and T2-weighted sequences, an iPAT (GRAPPA) factor of 2 and fat saturation were used.

The diffusion-weighted acquisition was a simultaneous multi-slice (SMS) accelerated, high-resolution spin-echo echo-planar imaging (SE-EPI) sequence with read-out segmentation of long variable echo trains (RESOLVE), parallel imaging and a two-dimensional navigator-based reacquisition, recorded at a TR of

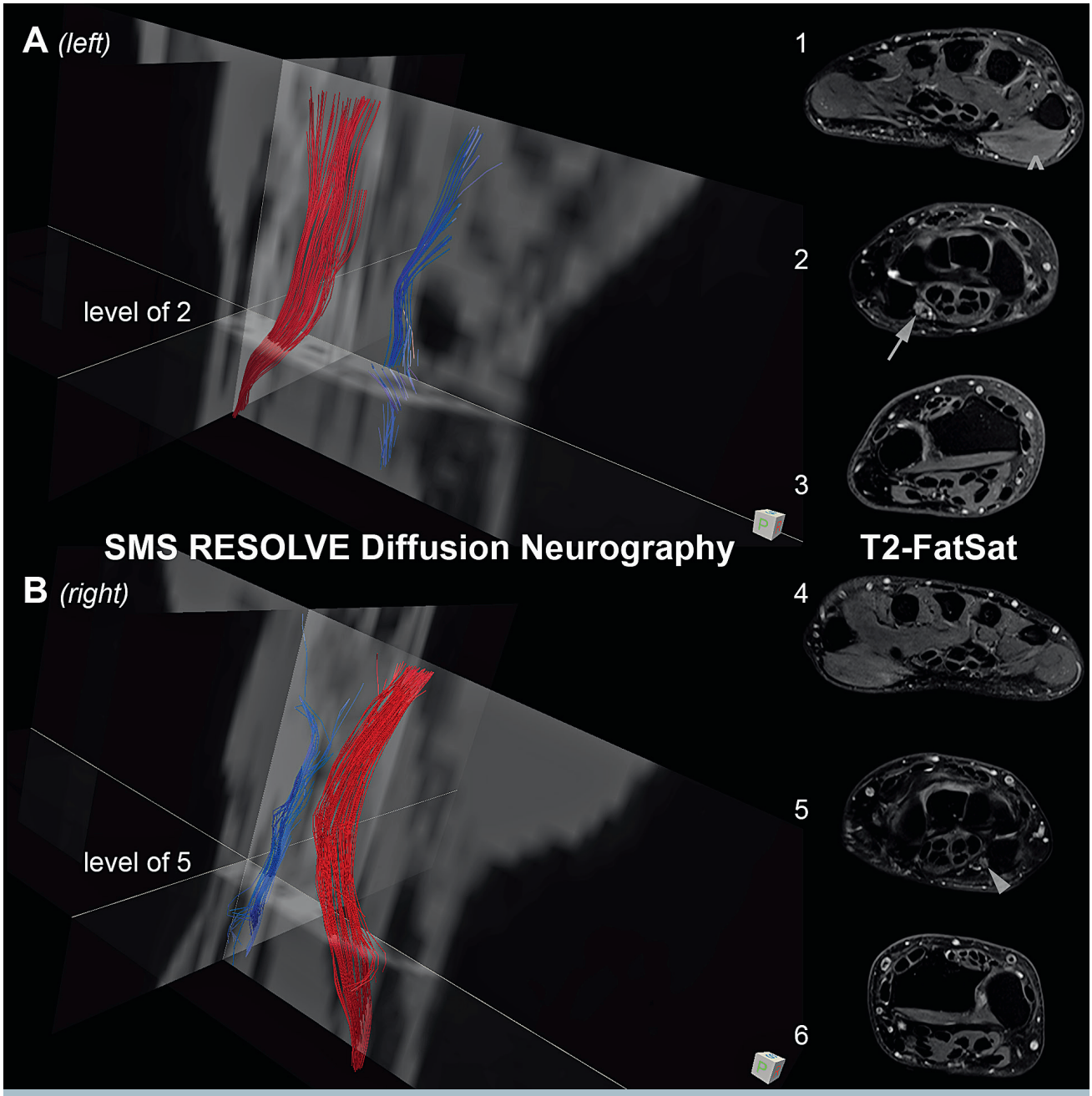

High-resolution SMS diffusion neurography in a patient with Loge-de-Guyon syndrome on the left. At the level of the left ulnar canal, fiber tracking was discontinuous and an increased angle threshold of interpolated streamlining was required to reconstruct the nerve. T2-weighted, fat-saturated imaging reveals focal hyperintensity and cross-sectional enlargement of the left ulnar nerve (arrow) compared to the right (arrowhead), consistent with distal ulnar compression neuropathy. (Note T2-hypointense flow void of the ulnar artery and T2-hyperintense ulnar veins, unambiguously allocated by T1-weighted contrast-enhanced images [not shown], in Guyon's canal on both sides.) Denervation edema of left thenar muscles normally innervated by the median nerve (abductor pollicis brevis and opponens pollicis) is also detected (caret), consistent with an innervation variant.

3000 ms, a TE of 50 ms, with a single measurement and 7 read-out segments, a SMS factor of 3, using monopolar diffusion-sensitizing gradients and 12 diffusion directions – isotropically distributed on the full sphere (generated using an optimization for eddy-current correction by gps, version 1.0, part of FSL, *http://fsl.fmrib.ox.ac.uk/fsl/fslwiki/*, see below) – at b = 800 s/mm^2 and with one b_0-image with no diffusion weighting, 7/8 partial Fourier sampling, at a pixel bandwidth of 868 Hz/pixel, a flip angle of 180°, with a field-of-view (FOV) of 94 mm x 75%, an effective matrix size of 80 x 60, resulting in an in-plane resolution of 1.18 x 1.18 mm, within a total acquisition time (TA) of 5.03 minutes.

The T2-weighted acquisition was a turbo-spin echo (TSE) sequence, recorded at a TR of 3000 ms, a TE of 95 ms, with 3 averages, an echo-train length of 11, a pixel bandwidth of 250 Hz/pixel, a flip angle of 120°, with a FOV of 100 mm x 60%, an effective matrix size of 256 x 152, resulting in an in-plane resolution of 0.39 x 0.39 mm, within a TA of 2.02 minutes.

Diffusion image post-processing was performed using tools from the Oxford Centre for Functional Magnetic Resonance Imaging of the Brain's Software Library (FMRIB Software Library FSL, version 5.0.9; *http://www.fmrib.ox.ac.uk/fsl*) [3] and consisted of (1) eddy current correction using eddy (part of FSL; [4]), (2) mask generation using fslmaths and fslview (version 3.2.0; both also part of FSL) and diffusion-tensor fitting with least squares using dtifit (again part of FSL).

Interpolated streamline diffusion neurography was performed using DiffusionToolkit (Version 0.6.3) and TrackVis (Version 0.6.0.1; *http://trackvis.org/*), using the default angle threshold of 35° (except for the Loge-de-Guyon segment of the left ulnar nerve, see below) and user-supplied masks (not shown) for seeding.

For comparison of the affected and unaffected side, both wrists were examined (Fig. 1A & 1B). On the affected left side (Fig. 1A), three cross-sectional seeds of the ulnar nerve – placed at the level of the Loge de Guyon (Fig. 1A – level of 2) as well as 15 mm proximally and distally to it – were required to reconstruct ulnar nerve fibers (displayed in blue-to-purple colors). Furthermore, the angle threshold had to be increased at the level Guyon's canal to enable fiber tracking on the left (90° were used here). On the unaffected right side (Fig. 1B), a single cross-sectional seed of the ulnar nerve – placed at the level of the Loge de Guyon (Fig. 1B – level of 5) – and the default angle threshold were sufficient for ulnar diffusion neurography (shown in blue). For the median nerve (fibers shown in red), a single cross-sectional seed at the level of the carpal tunnel and the default angle threshold were sufficient on both sides for diffusion neurography.

Imaging findings

At the level of the Loge de Guyon, the left ulnar nerve revealed the following pathological changes on MR neurography (MRN):

- Increased signal of all fascicles on the high-resolution T2-weighted, fat suppressed sequence compared to the ipsilateral median nerve and the nerves of the contralateral wrist (Fig. 1A, arrow at 2),
- focally increased ('pseudoneuroma-alike') cross-sectional area by 38% compared to the ulnar nerve of the contralateral wrist (Fig. 1A & 1B, 2 vs. 5),
- decreased mean fractional anisotropy (FA) value by 43% compared to the ulnar nerve of the contralateral wrist (not shown),
- decreased and discontinuous 'trackability' compared to the ulnar nerve of the contralateral wrist (Fig. 1A vs. 1B), as evidenced by:
  a) Interruption of fiber trackings at the level of the Loge de Guyon (three seeds were required to track the left ulnar nerve) and
  b) increased uncertainty of fiber orientations (an increased angle threshold had to be chosen at the level of Guyon's canal; see Imaging Sequence and Post-Processing Details above).

These findings are consistent with distal ulnar compression neuropathy due to a Loge-de-Guyon syndrome.

Furthermore, there was increased signal of the left abductor pollicis brevis and opponens pollicis muscles consistent with denervation edema (Fig. 1A, caret at 1) but atypical for ulnar neuropathy because these muscles are typically innervated by the median nerve (see Discussion).

Discussion

Peripheral neuropathies constitute a significant source of debilitating morbidity, and focal compressions of peripheral nerves are one of the frequent etiologies. Median nerve neuropathy due to compression in the carpal tunnel and ulnar nerve neuropathy due to compression in the cubital tunnel are most common while compression of the ulnar nerve at the level of the Loge de Guyon is less frequent.

The MR anatomy of the ulnar canal or Loge de Guyon has been described in detail [5]. Guyon's canal is formed between the pisiform and hamate by the superficial flexor retinaculum, i.e. the volar carpal ligament or ligamentum carpi palmare (palmar margin), the deep flexor retinaculum, i.e. the transverse carpal ligament or ligamentum flexorum (latero-dorsal margin), and the flexor carpi ulnaris along with the pisiform (ulnar margin). It contains the ulnar nerve, artery and vein (Fig. 1A & 1B, 2 & 5). Originating from the medial cord of the brachial plexus, the ulnar nerve enters Guyon's canal medial (ulnar) to the ulnar artery, superficial to the deep flexor retinaculum and proximal to the pisiform (zone 1). Within the Loge de Guyon, it bifurcates at the level of the distal pisiform into superficial sensory and deep motor branches dorso-medially to the hook of the hamate (zone 2). The motor branches normally supply the abductor (et flexor) and opponens digiti minimi, flexor carpi ulnaris, the ulnar part of the flexor digitorum profundus (IV et V), interossei, adductor pollicis, and fourth (and third) lumbricals as well as the palmaris brevis. Sensory branches pass superficially to supply the skin of the hypothenar eminence, the fifth and the medial aspect of the fourth digit (zone 3). Thus, zone 1 contains both motor and sensory fibers. Here, compression typically results in both motor and sensory changes. Compression of deep motor branches in zone 2 distal to the bifurcation results in pure motor deficits, prolonged distal motor latencies to and eventually atropy of the first dorsal interosseous and abductor digiti minimi, with no sensory changes. Compression of

superficial branches only in zone 3, resulting in pure sensory changes without motor deficits, are rare.

Compression can be due to fractures or fragments of the hook of the hamate, flexor tenosynovitis, atypical muscle bellies (esp. of the flexor digiti minimi brevis or abductor digiti minimi), space-occupying lesions including ganglion cysts from degenerative wrist disease or rheumatoid arthritis, lipomas or vascular pathologies such as (pseudo-) aneurysms of the ulnar artery or thrombosis. Compression can also result from chronic or repeated external pressure by push-ups, bicycle handle bars or, like in the presented case, from using crutches. Primary treatment consists of compression protection and, in refractory cases, of decompressive surgery. Regeneration tends to be slower and less successful for the ulnar compared to the median nerve.

High-resolution, fat-satured pulse sequences sensitive to prolonged T2-relaxation times constitute the gold standard to detect neuropathic changes by MRN. However, diffusion MRI of peripheral nerves and derived parameter maps of fractional anisotropy (FA), radial (RD) and axial (AD) diffusivity from diffusion tensor imaging (DTI) have already been shown to correlate distinctly with electrophysiological parameters (distal motor latencies, nerve conduction velocities and compound muscle action potentials) even in clinically asymptomatic individuals and to improve diagnostic accuracy in detecting peripheral neuropathy in conjunction with T2-weighted fat-satured imaging [6-8]. Previous studies were limited by in-plane resolutions and slice thicknesses, in particular, susceptible to profound partial volume contamination effects.

At a slice thickness of 4.0 mm and an interslice gap of 30% [6-8], peripheral nerve lesions of ≤1.2 mm may entirely fall into the gap and those ≤5.2 mm [!] are likely to be contaminated by partial volume effects of unaffected nerve tissue. In both situations, the measured FA values will be artificially increased which can lead to false-negative detections. At a low in-plane resolution, on the other hand, a thin peripheral nerve surrounded by fatty tissue in a canal, such as the cubital tunnel, will be contaminated by partial volume effects of tissue with no preference in the diffusion direction which will in turn artificially decrease the measured FA values. This situation can then lead to false-positive detections of 'abnormal' DTI parameters. For these reasons, a high spatial resolution, as offered by SMS RESOLVE, is essential to improve the diagnostic value of diffusion neurography of peripheral nerves.

High-resolution SMS RESOLVE now offers an unprecedented spatial resolution at low echo times and large coverage for diffusion neurography at clinically acceptable acquisition times to further improve its diagnostic performance. Such technology may also be instrumental to eventually detect previously unnoticed ischemic changes within peripheral nerves. Our case report illustrates the clinical utility of high-resolution SMS RESOLVE diffusion neurography in a patient with Loge-de-Guyon syndrome. Consistent with distal ulnar compression neuropathy, T2-weighted signal and cross-sectional area of the ulnar nerve was increased on the affected side while FA was profoundly decreased compared to the unaffected side. Streamline fiber tracking was impaired and discontinuous at the level of Guyon's canal (Fig. 1). As yet, very few studies have successfully reconstructed fiber pathways of peripheral nerves by diffusion neurography (emphasizing the high quality of our SMS RESOLVE data). Note that 'tractography' would be a misnomer in the peripheral nervous system.

Interestingly, there was denervation edema in thenar muscles normally supplied by the median nerve. Given that the median nerve showed no evidence of neuropathy, which virtually precludes muscular denervation due to median nerve lesions [9], this suggests (co-)innervation of the abductor pollicis brevis et opponens pollicis by the ulnar nerve in this particular case. Appreciation and recognition of innervation variants, such as the Martin-Gruber anastomosis between the median and ulnar nerve or the Riche-Cannien anastomosis between the median nerve and deep ramus of the ulnar nerve, are essential to interpret such 'paradoxical' changes. Atypical nerve supply ranges from partial or total innervation of the opponens pollicis and abductor pollicis brevis by the ulnar nerve as a mild form [10] to the rare 'all ulnar' or 'all median' hand in the extremes [11]. The latter are more frequent in dysmelias.

Conclusion

Here, two recent advances in the development of MRI pulse sequences, namely diffusion EPI using read-out segmentation of long variable echo trains (RESOLVE) and simultaneous multi-slice (SMS) imaging, have been combined for diffusion neurography of peripheral nerves in a case with Loge-de-Guyon syndrome. At present, diffusion neurography has a primarily confirmatory diagnostic value. However, with this exciting progress in pulse sequence development diffusion neurography is now feasible at high-resolution, reduced partial voluming (due to reduced slice thicknesses), relatively large coverage and low echo-times in clinically acceptable scan times. This is anticipated to promote application and early diagnostic value of diffusion neurography in the peripheral nervous system.

Acknowledgement

... to Siemens Healthcare GmbH, Germany (Wei Liu, Thorsten Feiweier, Heiko Meyer and Thomas Illigen, in particular), for excellent support.

... to the Oxford Centre for Functional MRI of the Brain (FMRIB) for the outstanding image processing software (FSL) they are developing.

... to Optoacoustics', Israel (http://www.optoacoustics.com/), Active Noise Cancellation (ANC) system to cancel out EPI read-out noise making diffusion neurography much more comfortable.

References

1 Porter DA, Heidemann R. High Resolution Diffusion-Weighted Imaging Using Readout-Segmented Echo-Planar Imaging, Parallel Imaging and a Two-Dimensional Navigator-Based Reacquisition. Magn Res Med 2009; 62:468-475.

2 MAGNETOM Flash 2015; 63 (3, supplement issue on Simultaneous Multi-Slice Imaging): 2-110.

3 Smith SM, Jenkinson M, Woolrich MW, Beckmann CF, Behrens TEJ, Johansen-Berg H, et al. Advances in functional and structural MR image analysis and implementation as FSL. Neuroimage 2004; 23(Suppl 1): S208-219.

4 Anderson, J. L. R. (2014). Geometric distortions in diffusion MRI. In: Diffusion MRI: from quantitative measurement to in-vivo neuroanatomy. Johansen-Berg, H. & Behrens, T. E. (Eds.), 2nd edition, Elsevier Academic Press, Amsterdam (ISBN 978-0-12-396460-1), 2014. pp. 63-85.

5 Zeiss J, Jakab E, Khimji T, Imbriglia J. The ulnar tunnel at the wrist (Guyon'scanal): normal MR anatomy and variants. AJRAmJRoentgenol 1992, 158(5):1081-5.

6 Baeumer P, Pham M, Ruetters M, Heiland S, Heckel A, Radbruch A, et al. Peripheral Neuropathy: Detection with Diffusion-Tensor Imaging. Radiology 2014, 273(1):185-193.

7 Heckel A, Weiler M, Xia A, Ruetters M, Pham M, Bendszus M, et al. Peripheral Nerve Diffusion Tensor Imaging: Assessment of Axon and Myelin Sheath Integrity. PLOS One 2015, 10(6):e0130833.

8 Breckwoldt MO, Stock C, Xia A, Heckel A, Bendszus M, Pham M, et al. Diffusion Tensor Imaging Adds Diagnostic Accuracy in Magnetic Resonance Neurography. Invest Radiol. 2015 Aug;50(8):498-504.

9 Schwarz D, Weiler M, Pham M, Heiland S, Bendszus M, Bäumer P. Diagnostic signs of motor neuropathy in MR neurography: nerve lesions and muscle denervation. Eur Radiol 2015;25(5):1497-1503.

10 von Lanz, T, Wachsmuth, W, Praktische Anatomie. Arm (1. Band, 3. Teil, 2. Auflage). Springer, Berlin, 1959. pp. 36-44, 214.

11 Broser, F, Topische und klinische Diagnostik neurologischer Krankheiten (2. Auflage). Urban & Schwarzenberg, München, 1981. Pp. 49-50, 60-62.

Contact

Andreas Joachim Bartsch, MD
Radiologie Bamberg
http://www.radiologie-bamberg.de/
Heinrichsdamm 6
96047 Bamberg
Germany
bartsch@radvisory.net

Further Information

For MR Neurography protocols, case studies, clinical articles and expert talks please visit us at **www.siemens.com/MR-Neurography**